Journal of Theoretical Biology 266 (2010) 408–418

Contents lists available at ScienceDirect

Journal of Theoretical Biology

journal homepage: www.elsevier.com/locate/yjtbi

Feedback-control induced pattern formation in cardiac myocytes: A mathematical modeling study ☆

Stephen A. Gaeta, Trine Krogh-Madsen, David J. Christini *

Greenberg Division of Cardiology, Department of Physiology, Biophysics and Systems Biology, Weill Cornell Medical College, 1300 York Ave., New York, NY 10065, USA

ARTICLE INFO

Article history:
Received 12 February 2010
Received in revised form
8 June 2010
Accepted 29 June 2010
Available online 8 July 2010

Keywords:
Cardiac electrophysiology
Alternans
Subcellular alternans
Arrhythmia

ABSTRACT

Cardiac alternans is a dangerous rhythm disturbance of the heart, in which rapid stimulation elicits a beat-to-beat alternation in the action potential duration (APD) and calcium (Ca) transient amplitude of individual myocytes. Recently, "subcellular alternans", in which the Ca transients of adjacent regions within individual myocytes alternate out-of-phase, has been observed. A previous theoretical study suggested that subcellular alternans may result during static pacing from a Turing-type symmetry breaking instability, but this was only predicted in a subset of cardiac myocytes (with negative Ca to voltage ($Ca \rightarrow V_m$) coupling) and has never been directly verified experimentally. A recent experimental study, however, showed that subcellular alternans is dynamically induced in the remaining subset of myocytes during pacing with a simple feedback control algorithm ("alternans control"). Here we show that alternans control pacing changes the effective coupling between the APD and the Ca transient ($V_m \rightarrow Ca$ coupling), such that subcellular alternans is predicted to occur by a Turing instability in cells with positive $Ca \rightarrow V_m$ coupling. In addition to strengthening the understanding of the proposed mechanism for subcellular alternans formation, this work (in concert with previous theoretical and experimental results) illuminates subcellular alternans as a striking example of a biological Turing instability in which the diffusing morphogens can be clearly identified.

© 2010 Elsevier Ltd. All rights reserved.

1. Introduction

Cardiac alternans is a disturbance in the rhythm of the diseased heart that predisposes to the formation of potentially fatal arrhythmias and serves clinically as an indicator of likelihood of sudden cardiac death. Alternans is seen clinically on the electrocardiogram (ECG) during rapid heart rates, when consecutive T-waves on the ECG alternate in amplitude (Narayan, 2006). This "T-wave alternans" is known to be a manifestation of underlying beat-to-beat alternations in the action potential durations (APDs) and peak intracellular calcium (Ca) concentrations of individual cardiac myocytes (Fig. 1A). Although alternans has been mechanistically linked to the formation of potentially fatal reentrant arrhythmias (e.g. ventricular tachycardia/fibrillation) (Pastore et al., 1999), its underlying mechanism remains unclear. Treatment or prevention of alternans may serve as a useful strategy for precluding its dangerous consequences, but no clinically practical means of doing so currently exist.

Alternans at the cellular level is understood to result from the interplay of ion channels at the cell surface and the dynamics of intracellular calcium cycling that are responsible for the rise in calcium concentration seen with each beat. Uncertainty still remains, however, regarding the primary source of instability that leads the normally period-1 rhythm (in which consecutive APDs and Ca transient amplitudes do not vary) to become a period-2, alternans rhythm at fast pacing cycle lengths (Fig. 1A). Theoretical and experimental work has identified mechanisms by which APD-alternans and Ca-alternans can result independently from one another, due only to instability in sarcolemmal ion channel and intracellular Ca-cycling dynamics, respectively. Due to bidirectional coupling between the APD and the Ca transient (described below), however, alternans in the APD will cause secondary alternans in the amplitude of intracellular Ca transients, and vice versa. This has made determination of the primary source of instability a difficult experimental challenge (Jordan and Christini, 2007; Qu and Weiss, 2007). Although Ca-cycling dynamics are now generally accepted as the primary cause of alternans (so-called "Ca-driven" alternans), both are likely to contribute to the total instability seen (Weiss et al., 2006).

Each Ca transient within a cardiac myocyte is the result of 1000s of nearly simultaneous, discrete subcellular Ca release events (Franzini-Armstrong and Peachey, 1981; Cheng and Lederer, 2008), which together result in an approximately

☆ Funded by: NIH.

* Corresponding author. Tel.: +1 212 746 6280; fax: +1 212 746 6669.
E-mail addresses: stg2004@med.cornell.edu (S.A. Gaeta), trk2002@med.cornell.edu (T. Krogh-Madsen), dchristi@med.cornell.edu (D.J. Christini).

0022-5193/$ - see front matter © 2010 Elsevier Ltd. All rights reserved.
doi:10.1016/j.jtbi.2010.06.041

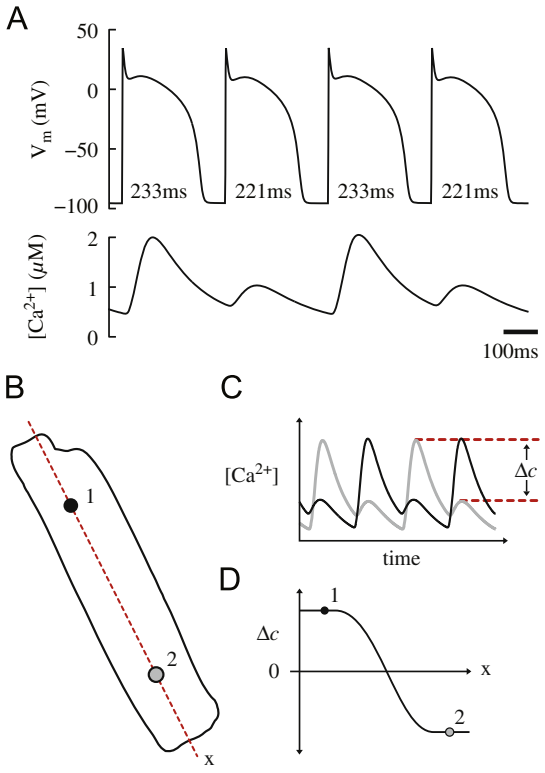


Fig. 1. (A) Alternans manifests at the cellular level as beat-to-beat alternations in the duration of subsequent action potentials (top) and the amplitude of consecutive intracellular Ca transients (bottom). Traces shown are from the detailed ionic model (see "Computational model" section for description), paced at a constant cycle length of 300 ms. The APD, defined as the time to 90% repolarization, is shown for each action potential. (B–D) Subcellular alternans occurs when distinct subcellular regions of an individual myocyte exhibit Ca-alternans of opposite phase (as diagrammed for regions 1 and 2; C). (D) This is simplified here as the formation of a gradient in Ca-alternans magnitude (Δc), where Δc is defined as the difference in peak Ca concentration between subsequent Ca transients (C; Eq. (18)). A 2-region subcellular alternans is diagrammed in this example, in which Ca transients in the two halves of the cell alternate out-of-phase, separated by a "node" with period-1 (no alternans) Ca transients where $\Delta c = 0$. B–D adapted with permission from Y. Shiferaw.

spatially synchronized change in intracellular Ca concentration. Likewise, during alternans the intracellular Ca transient normally remains spatially synchronized, with uniform alternations in Ca concentration within an individual cell. Recently, however, so-called "subcellular alternans" has been reported, in which the Ca transient desynchronizes spatially, and Ca-alternans occurs with opposite phase in adjacent subcellular regions of a single cell (as in Figs. 1B, C, and 4C) (Aistrup et al., 2006, 2009; Cordeiro et al., 2007; Díaz et al., 2002, 2004; Gaeta et al., 2009; Kapur et al., 2009; Karma and Gilmour, 2007; Kockskämper and Blatter, 2002; Xie and Weiss, 2009). This most commonly manifests as the two halves of an individual cell exhibiting beat-to-beat alternation in Ca transient amplitude, but with one half experiencing large–small–large Ca transients while the other half experiences small–large–small transients.

Although this phenomenon remains poorly characterized, several studies have shown its arrhythmogenic potential as a cause of intracellular waves of Ca-release ("Ca waves"), which are known to contribute to after depolarizations and triggered activity (Kockskämper and Blatter, 2002; Díaz et al., 2004, 2002; Xie and Weiss, 2009). Several mechanisms have been proposed to account for the formation of subcellular alternans during rapid pacing of otherwise healthy cells, invoking either anatomical (Aistrup et al., 2009) or dynamically induced (Xie and Weiss, 2009; Shiferaw and Karma, 2006) heterogeneity in subcellular Ca-cycling characteristics.

A recent theoretical study suggested that a purely dynamical mechanism—a Turing-type instability—can induce subcellular alternans in a structurally homogeneous cell (Shiferaw and Karma, 2006). A canonical Turing ("diffusion-driven") instability is a mechanism by which a concentration gradient can be established from a nearly homogenous substrate due to the interaction of only two distinct, diffusing substances ("morphogens") (Turing, 1952). This occurs when an autocatalytic substance ("activating morphogen") gives rise to its own, more quickly diffusing inhibitor ("inhibitory morphogen"). A concentration gradient arises because local increases in activator concentration will grow (autocatalysis) but will also simultaneously inhibit increases in activator concentration away from this site (due to the production of the more quickly diffusing inhibitor) (Gierer and Meinhardt, 1972). Since it was first proposed in 1952 by Turing (1952), this well-characterized, generic mechanism of pattern-formation has been invoked many times to account for patterns seen in systems as diverse as coat patterns in mammals (Murray, 2003) and shell patterns in mollusks (Meinhardt and Gierer, 2000), but the complexity of biological systems makes clear identification of the interacting morphogens difficult.

The previous study drew an elegant analogy between the amplitudes of Ca-alternans and APD-alternans and the concentrations of the activating and inhibitory morphogen in a canonical Turing instability (Shiferaw and Karma, 2006). By defining the "Ca-alternans amplitude" (Δc) as the difference in peak calcium concentration of consecutive beats at each point along the length of a cell, subcellular alternans was able to be treated as the formation of a stable gradient in Δc along the length of the cell. For example, if on two consecutive beats the left half of a myocyte experiences a small Ca-transient followed by a large transient concurrent with the right half having a large followed by a small transient (subcellular alternans), Δc will be positive on the left and negative on the right (as seen in Figs. 1D, 4B, and C).

Using a simplified coupled-map model, it was shown that such a gradient (subcellular alternans) will arise by a Turing-type instability given proper coupling between the AP and the Ca-transient. In particular, subcellular alternans was predicted to form by this mechanism during static (constant cycle length) pacing of only an uncommon subset of cardiac myocytes—those in which the Ca transient amplitude is negatively coupled to the APD ("negative $Ca \rightarrow V_m$ coupling", defined below). Here we show that this mathematical analysis also predicts that subcellular alternans will result in the remaining, more common subset of myocytes (those with positive $Ca \rightarrow V_m$ coupling, defined below) during pacing with a simple feedback control algorithm, "alternans control". Indeed, we have recently shown (in both a computational model and isolated guinea pig ventricular myocytes) that alternans control pacing robustly induces subcellular alternans in such cells (Gaeta et al., 2009). The mathematical and computational modeling work herein defines the theoretical basis for the subcellular alternans seen in those experiments, and identifies an intriguing experimental utility for alternans control pacing in the future study of alternans mechanisms.

2. Theory

2.1. Sarcomere model

To explore the effects of coupling between APD and intracellular calcium transients, Shiferaw and Karma (2006) introduced a

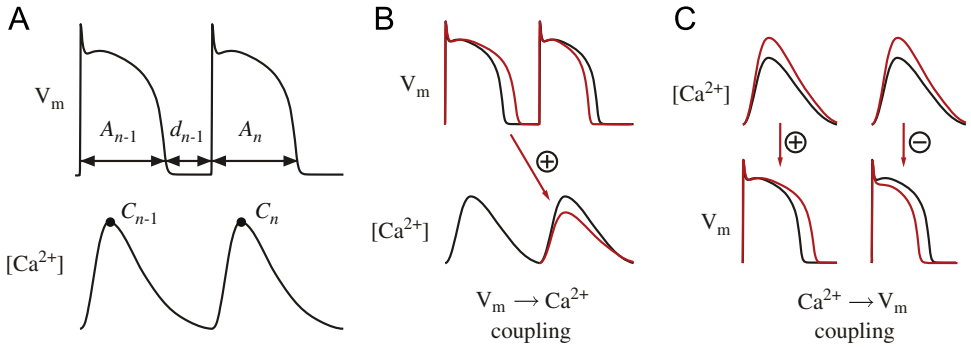


Fig. 2. (A) In the 2-dimensional coupled map model of a sarcomere, the APD of beat n (A_n) is a function of the preceding APD (A_{n-1}) as well as the peak concentration of the concurrent Ca transient (C_n). Likewise, the peak Ca concentration of beat n (C_n) is a function of both the preceding APD (A_{n-1}) and the peak Ca concentration of the preceding beat (C_{n-1}). (B) During static pacing, $V_m \rightarrow Ca$ coupling is assumed to be positive due to graded release (as shown). An increase in the preceding APD leads to a decrease in the subsequent Ca transient (due to a shortening of the diastolic interval), and vice versa. (C) $Ca \rightarrow V_m$ coupling can be either positive (left) or (negative), dependent on species, cell type, and temperature.

2-dimensional coupled map of a sarcomere in which

$$A_n = F_1(A_{n-1}, C_n),$$

$$C_n = F_2(A_{n-1}, C_{n-1}), \tag{1}$$

where A_n is the APD and C_n the peak Ca concentration for beat n (Fig. 2A) (Shiferaw and Karma, 2006). Note that this type of map has been used before to explore the dynamics of entire cells (in which the cell was considered homogeneous) (Qu et al., 2007), but here is taken to represent the dynamics on the level of individual sarcomeres.

As detailed below, in this simplified model, the APD of a given beat is a function of both the preceding APD (due, implicitly, to APD restitution; see below) and the concurrent Ca-transient (due to the effects of Ca-sensitive membrane currents ("$Ca \rightarrow V_m$ coupling"). Similarly, the magnitude of each beat's Ca transient is a function of the preceding APD ("$V_m \rightarrow Ca$ coupling") and the preceding Ca transient (due to, for instance, depletion of sarcoplasmic reticulum Ca stores; Shiferaw et al., 2003). These dependencies are reflected in the Jacobian matrix (J) of this model,

$$J = \begin{pmatrix} \dfrac{\partial A_n}{\partial A_{n-1}} + \dfrac{\partial A_n}{\partial C_n}\dfrac{\partial C_n}{\partial A_{n-1}} & \dfrac{\partial A_n}{\partial C_n}\dfrac{\partial C_n}{\partial C_{n-1}} \\ \dfrac{\partial C_n}{\partial A_{n-1}} & \dfrac{\partial C_n}{\partial C_{n-1}} \end{pmatrix}, \tag{2}$$

which describes the behavior of this model close to its period-1 fixed point (A^*, C^*).

The previous study used this sarcomere model to derive a spatially extended (reaction–diffusion) model of an entire myocyte (Shiferaw and Karma, 2006), in which a 1-dimensional cable of such sarcomeres are coupled by voltage and Ca diffusion. As described below, they showed the sign of the elements of J (describing the coupling characteristics of each individual sarcomere) to have important effects on the stability of the whole-cell model, including the formation of subcellular alternans.

2.1.1. APD restitution

In the above sarcomere model, the dependence of each APD on that of the preceding beat ($\partial A_n/\partial A_{n-1}$) implicitly models the effect of so-called "APD restitution", which dictates that a shortened diastolic interval (d_n) will be followed by a shortened subsequent APD (A_{n+1}), and vice versa. With static pacing, during which $T = A_n + d_n$ (where T is a constant cycle length), prolonging a given APD will shorten the following diastolic interval, thereby causing a shortened subsequent APD. This was included in the previous study by the assumption that $\partial A_n/\partial A_{n-1} < 0$, but here, we will explicitly include the effect of the diastolic interval by expanding this definition to

$$\frac{\partial A_n}{\partial A_{n-1}} \equiv \frac{\partial A_n}{\partial d_{n-1}}\frac{\partial d_{n-1}}{\partial A_{n-1}}, \tag{3}$$

where $\partial A_n/\partial d_{n-1}$ describes APD restitution and is assumed to be positive (reflecting a monotonic APD restitution curve). Note that during static pacing $\partial d_n/\partial A_n = -1$, and the above quantity remains negative (as was assumed in the previous study). These intrinsic V_m–dynamics can lose stability ($\partial A_n/\partial A_{n-1} < -1$) when APD restitution is sufficiently steep ($\partial A_n/\partial d_{n-1} > 1$), thereby resulting in APD-alternans.

2.1.2. Voltage to calcium coupling

Likewise, the dependence of each beat's peak Ca concentration on the preceding APD ($\partial C_n/\partial A_{n-1}$; "$V_m \rightarrow Ca$ coupling") implicitly models the effect of so-called "graded release", which dictates that a shorter diastolic interval (d_n) will give rise to a smaller subsequent Ca transient (C_{n+1}), and vice versa. In the previous study (Shiferaw and Karma, 2006), this was included by the assumption that $\partial C_n/\partial A_{n-1} < 0$, which states that a prolongation of the preceding APD (A_{n-1}) will cause a decrease in the subsequent calcium transient (C_n), and vice versa. This relationship is denoted "positive $V_m \rightarrow Ca$ coupling" and is a consistent experimental observation (Fig. 2B). Note that given positive $V_m \rightarrow Ca$ coupling, alternans in the APD will cause in-phase secondary Ca-alternans.

To explicitly model the effects of the diastolic interval on this coupling, here we will expand this definition to

$$\frac{\partial C_n}{\partial A_{n-1}} \equiv \frac{\partial C_n}{\partial d_{n-1}}\frac{\partial d_{n-1}}{\partial A_{n-1}}, \tag{4}$$

where $\partial C_n/\partial d_{n-1}$ reflects graded release and is assumed to be positive. Note that during static pacing (when $\partial d_n/\partial A_n = -1$, as above), Eq. (4) predicts positive $V_m \rightarrow Ca$ coupling ($\partial C_n/\partial A_{n-1} < 0$), as was assumed in the previous study.

2.1.3. Calcium to voltage coupling

Similarly, changes in intracellular Ca concentration can be positively or negatively coupled to V_m (and thereby APD) through the opposing effects of the sodium–calcium exchanger (NCX) and Ca-induced inactivation of L-type Ca channels (Fig. 2C).

So-called "positive $Ca \rightarrow V_m$ coupling" occurs when the depolarizing effect of NCX Ca extrusion is stronger than the hyperpolarizing effect of Ca-induced inactivation of L-type Ca channels. In this case, an increase in intracellular Ca concentration has a net depolarizing effect on the membrane voltage, and therefore prolongs the concurrent APD ($\partial A_n/\partial C_n > 0$). In a cell with positive $Ca \rightarrow V_m$ coupling, Ca-alternans will cause in-phase secondary APD-alternans

(electromechanically (EM) concordant alternans; Shiferaw et al., 2005).

Alternatively, if the effect of Ca-induced inactivation of L-type Ca channels outweighs that of the NCX, changes in intracellular Ca concentration will be negatively coupled to V_m. In this case, an increase in intracellular Ca concentration has a net hyperpolarizing effect on the membrane voltage, and will therefore shorten the concurrent APD ($\partial A_n/\partial C_n < 0$), and Ca-alternans will cause out-of-phase secondary APD-alternans (EM discordant alternans; Shiferaw et al., 2005).

Both EM discordant and, more commonly, EM concordant alternans have been seen experimentally as a species, cell type, and (in some cases) temperature dependent characteristic (Rubenstein and Lipsius, 1995; Euler, 1999).

2.2. Conditions for a turing-type instability

The previous study (Shiferaw and Karma, 2006) modeled the spatiotemporal dynamics of APD-alternans and Ca-alternans by defining each as a small amplitude oscillation about the period-1 fixed point (A^*, C^*), given by

$$A_n = A^* + (-1)^n a(n), \tag{5}$$

$$C_n = C^* + (-1)^n c(n), \tag{6}$$

where $a(n)$ and $c(n)$ represent the amplitudes of APD-alternans and Ca-alternans, respectively. Note that with this definition, alternans amplitudes of opposite sign indicate alternans of opposite phase.

As detailed in Shiferaw and Karma (2006), this simple model of alternans amplitudes in an individual sarcomere was used to derive a continuous reaction–diffusion model describing the evolution of small amplitude alternans (near the alternans bifurcation) in an entire myocyte, modeled as a 1-dimensional cable of identical sarcomeres coupled by diffusion of voltage and Ca between adjacent points in the cell. The derived amplitude equations were

$$\frac{\partial a}{\partial t} = \alpha a + \beta \bar{c},$$

$$\frac{\partial c}{\partial t} = \gamma a + \mu \bar{c} + \delta c + D\partial_x^2 c, \tag{7}$$

where $\bar{c} = (1/L)\int_0^L c(x,t)\,dx$, and Ca-alternans amplitude spreads to adjacent sarcomeres with an effective diffusion constant D. Note that APD-alternans (a) does not have a diffusion term, due to an approximation of instantaneous voltage diffusion. Importantly, the constant coefficients in this reaction–diffusion system can be expressed in terms of the elements of the Jacobian of the original 2D map (Eq. (2)), allowing the conditions for stability at the whole-cell level (derived from Eq. (7)) to be expressed as requirements on the behavior of the individual sarcomeres (below).

In this model, subcellular alternans manifests as the formation of a gradient in Ca-alternans amplitude (c) along the length of the cell, in which Ca-alternans occurs with opposite phase (c's of opposite sign) in different regions of the same cell. Linear stability analysis of Eq. (7) showed that such a gradient can form by a Turing-type pattern forming instability if three conditions are met by the coupling between the APD and the Ca transient at the level of the individual sarcomere (Shiferaw and Karma, 2006). These are (1) $J_{22} < -1$ (i.e. Ca-cycling dynamics must be unstable), (2) $J_{22} < J_{11}$ (i.e. Ca-cycling dynamics must be more unstable (more negative) than V_m (APD) dynamics) and (3) $J_{12}J_{21} < 0$. Whereas the first two conditions describe so-called "Ca-driven" alternans (in which APD-alternans is secondary to Ca-alternans), which is thought to be the case for most cardiac myocytes (Weiss et al., 2006), the third condition places requirements on the specific coupling between the APD and the Ca transient that were shown to only be satisfied in cells with either

I. Positive $V_m \rightarrow Ca$ coupling and negative $Ca \rightarrow V_m$ coupling, or
II. Negative $V_m \rightarrow Ca$ coupling and positive $Ca \rightarrow V_m$ coupling,

as shown below. Because positive $V_m \rightarrow Ca$ coupling is normally assumed during static pacing (due to graded release, as described above), the previous analysis predicted subcellular alternans only in cells with negative $Ca \rightarrow V_m$ coupling (type I above; Shiferaw and Karma, 2006). Although negative $V_m \rightarrow Ca$ coupling is theoretically possible (Weiss et al., 2006), to the best of our knowledge it has never been reported experimentally.

Here we show that during pacing with a simple feedback-control algorithm ("alternans control"), $V_m \rightarrow Ca$ coupling can be effectively negative. Subcellular alternans is therefore predicted to occur by the same Turing-type instability in the previously excluded subset of cardiac myocytes (those with positive $Ca \rightarrow V_m$ coupling; type II, above) during alternans control pacing.

2.3. Alternans control

Alternans control is a well studied feedback-control pacing algorithm intended to exploit the dependence of APD on the preceding diastolic interval (APD restitution) to eliminate alternans (Christini et al., 2006; Hall and Christini, 2001; Hall and Gauthier, 2002). During alternans control pacing, the cycle length is recalculated following each action potential by the algorithm

$$T_n = T^* + g(A_n - A_{n-1}), \tag{8}$$

where T_n is the pacing cycle length of beat n, T^* is the target pacing cycle length, g is the control gain (assumed to be positive), and A_n is the APD of beat n (as above). To analyze the effects of alternans control pacing on the 2D model above, here we model the effect of alternans control as changes in the coupling of each APD (A_n) to the subsequent diastolic interval (d_n). The validity of this approach is evaluated in the Limitations section. Because $T_n = A_n + d_n$, Eq. (8) is equivalent to

$$d_n = T^* + g(A_n - A_{n-1}) - A_n. \tag{9}$$

Unlike during static pacing, in which $\partial d_n/\partial A_n = -1$ (as above), Eq. (9) shows that during alternans control pacing the change in diastolic interval for a given change in APD is

$$\frac{\partial d_n}{\partial A_n} = g - 1. \tag{10}$$

Note that alternans control without gain ($g=0$) is equivalent to static pacing. Alternans control pacing will thus affect both the instability of intrinsic APD dynamics (Eq. (3)) as well as $V_m \rightarrow Ca$ coupling (Eq. (4)). During alternans control pacing these relationships become

$$\frac{\partial A_n}{\partial A_{n-1}} = (g-1)\frac{\partial A_n}{\partial d_{n-1}}, \tag{11}$$

and

$$\frac{\partial C_n}{\partial A_{n-1}} = (g-1)\frac{\partial C_n}{\partial d_{n-1}}, \tag{12}$$

respectively.

Noting that $\partial A_n/\partial d_{n-1} > 0$ (APD restitution), Eq. (11) shows that alternans control pacing (with positive gain) stabilizes intrinsic APD-dynamics, as has been previously reported (Hall and Christini, 2001). Likewise, assuming graded release coupling ($\partial C_n/\partial d_{n-1} > 0$), Eq. (12) shows that during alternans control pacing, $V_m \rightarrow Ca$ coupling is effectively negative ($\partial C_n/\partial A_{n-1} > 0$) for

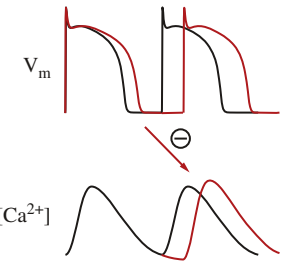


Fig. 3. During alternans control, if the gain is sufficiently high ($g>1$ in this model), $V_m \rightarrow Ca$ coupling is effectively negative, meaning an increase in the APD leads to an increase in the peak concentration of the subsequent calcium transient ($\partial C_n/\partial A_{n-1}>0$), and vice versa. This is contrary to static pacing, in which $V_m \rightarrow Ca$ coupling is assumed to be positive (as in Fig. 2B).

all $g>1$ (Fig. 3). To the best of our knowledge, this change in effective $V_m \rightarrow Ca$ coupling has not been previously reported.

Unlike $V_m \rightarrow Ca$ coupling, $Ca \rightarrow V_m$ coupling ($\partial A_n/\partial C_n$) occurs during the concurrent beat, and is therefore unaffected by the changes in diastolic interval during alternans control. Likewise, the feedback of calcium onto itself ($\partial C_n/\partial C_{n-1}$), is assumed to be mediated by diastolic interval independent mechanisms (e.g. depletion of SR calcium stored, and RyR refractoriness); intrinsic Ca-cycling instability is therefore unaffected by alternans control pacing in this analysis.

2.4. *Alternans control pacing is predicted to induce subcellular alternans in myocytes with positive* $Ca \rightarrow V_m$ *coupling and Ca-driven alternans*

Because the incorporation of these effects of alternans control pacing changes only the value of the dependencies described above, and not the structure of the model itself (or the reaction–diffusion system derived from it), the same three conditions for subcellular alternans formation found by the previous analysis are predicted to apply during alternans control pacing. By analyzing each of these conditions in turn, we find that they are indeed satisfied in myocytes with positive $Ca \rightarrow V_m$ coupling (and Ca-driven alternans), as follows.

The first condition, $J_{22}<-1$, corresponds physically to the condition that intrinsic Ca-cycling dynamics must be unstable. By Eq. (2), this condition is

$$\frac{\partial C_n}{\partial C_{n-1}}<-1. \tag{13}$$

As described above, this dependence reflects the feedback of calcium onto itself through non-diastolic interval dependent mechanisms; this condition is therefore unaffected by alternans control pacing in this analysis.

The second condition, $J_{22}<J_{11}$ dictates that the degree of Ca-cycling instability (J_{22}) must be greater (more negative) than the degree of V_m−instability (J_{11}). In other words, alternans must be primarily Ca-driven. From Eq. (2), this condition is

$$\frac{\partial C_n}{\partial C_{n-1}}<\frac{\partial A_n}{\partial A_{n-1}}+\frac{\partial A_n}{\partial C_n}\frac{\partial C_n}{\partial A_{n-1}}. \tag{14}$$

By Eqs. (11) and (12), during alternans control pacing this becomes

$$\frac{\partial C_n}{\partial C_{n-1}}<(g-1)\left[\frac{\partial A_n}{\partial d_{n-1}}+\frac{\partial A_n}{\partial C_n}\frac{\partial C_n}{\partial d_{n-1}}\right]. \tag{15}$$

Assuming $\partial A_n/\partial d_{n-1}>0$ (monotonic APD restitution) and $\partial C_n/\partial d_{n-1}>0$ (graded release), in a cell with positive $Ca \rightarrow V_m$ coupling ($\partial A_n/\partial C_n>0$) the bracketed quantity is always positive. In such a cell, the effect of alternans control pacing ($g>0$) is therefore to diminish APD-instability (make the right-hand side of Eq. (15) less negative). Importantly, if this condition is satisfied during static pacing ($g=0$), it will also be satisfied during alternans control pacing.

Finally, the third condition ($J_{12}J_{21}<0$) places requirements on the bidirectional coupling between the APD and the Ca transients. By Eq. (2), this condition is

$$\frac{\partial A_n}{\partial C_n}\frac{\partial C_n}{\partial C_{n-1}}\frac{\partial C_n}{\partial A_{n-1}}<0. \tag{16}$$

When $\partial C_n/\partial C_{n-1}<-1$ (condition 1), this condition simplifies to

$$\frac{\partial A_n}{\partial C_n}\frac{\partial C_n}{\partial A_{n-1}}>0. \tag{17}$$

Noting that $\partial A_n/\partial C_n$ represents $Ca \rightarrow V_m$ coupling and $\partial C_n/\partial A_{n-1}$ represents $V_m \rightarrow Ca$ coupling, this condition places requirements on the bidirectional coupling between membrane voltage (APD) and intracellular calcium. As described in Shiferaw and Karma (2006), this condition is satisfied in cells with either negative $Ca \rightarrow V_m$ coupling and positive $V_m \rightarrow Ca$ coupling ($\partial A_n/\partial C_n<0$, $\partial C_n/\partial A_{n-1}<0$; type I, above) or with positive $Ca \rightarrow V_m$ coupling and negative $V_m \rightarrow Ca$ coupling ($\partial A_n/\partial C_n>0$, $\partial C_n/\partial A_{n-1}>0$; type II, above).

We have found that during alternans control pacing (with sufficiently high gain), $V_m \rightarrow Ca$ coupling becomes effectively negative (Eq. (12)), thereby satisfying this condition in cells with positive $Ca \rightarrow V_m$ coupling (type II, above). Our analysis therefore predicts that subcellular alternans will be dynamically induced by the previously proposed Turing-type instability during alternans control pacing (with sufficiently high gain) in cells with positive $Ca \rightarrow V_m$ coupling and Ca-driven alternans.

3. Computational model

To test these predictions in a more realistic cell model, we implemented the detailed ionic model of Shiferaw and Karma (2006) (also used in Aistrup et al., 2009; Gaeta et al., 2009), in which a single myocyte is represented as a 1-dimensional chain of individual sarcomeres, each with its own Ca-cycling dynamics and Ca concentrations. In this model, membrane voltage is determined by the average states of all sarcomeres and is thus synchronized over the entire cell at all times. Sarcomeres are coupled to one another by compartment-specific Ca-diffusion and through bidirectional coupling with membrane voltage. For a detailed description of model formulation, see Shiferaw and Karma (2006).

Well characterized parameter adjustments to this model control both the sign of $Ca \rightarrow V_m$ coupling as well as the degree of V_m−driven and Ca-cycling instability (Shiferaw et al., 2003; Jordan and Christini, 2007). In particular, we tuned the model to exhibit positive $Ca \rightarrow V_m$ coupling by adjusting the sensitivity of L-type Ca channels to Ca-induced inactivation ($\gamma=0.7$). Additionally, the degree of V_m and Ca-driven instability were controlled by adjusting the time constant of recovery from inactivation of the L-type Ca channels (τ_f) and the load dependence of SR Ca release (u), respectively. Three different sets of parameters were used, corresponding to cell models in which alternans is primarily V_m−driven ($\tau_f=60$ ms and $u=5\,s^{-1}$), Ca-driven ($\tau_f=50$ ms and $u=13\,s^{-1}$), or driven by both V_m and Ca-cycling instability ("mixed-instability"; $\tau_f=40$ ms and $u=11\,s^{-1}$). The effects of these parameter adjustments have been previously characterized (Shiferaw and Karma, 2006; Jordan and Christini, 2007; Shiferaw et al., 2003).

4. Results

4.1. Subcellular alternans is induced in the positively coupled model during alternans control pacing

Using this model, we first assessed the effect of alternans control pacing on the stability of the period-1, spatially homogeneous state over a range of pacing cycle lengths. For each pacing cycle length, the spatially homogeneous, period-1 state was reached by static pacing while averaging all state variables at the beginning of each cycle with their values from the start of the preceding cycle. The state variables at the end of 300 beats were recorded and used as initial conditions in subsequent simulations. For each pacing cycle length (T^*), alternans control pacing was applied (according to Eq. (8)) with gains from 0.0 to 2.0, beginning from the spatially homogeneous period-1 state. Note that $g=0.0$ corresponds to static pacing. Gaussian white noise ($\sigma = 0.1\%$ of steady-state values) was added to all Ca concentrations at the time step before each stimulus. This protocol was repeated for the V_m−driven, Ca-driven, and mixed instability cell model at pacing cycle lengths of 200–400 ms.

An example of these simulations is seen in Fig. 4, in which the evolution of APD-alternans amplitude (ΔA) and Ca-alternans amplitude (Δc) for each sarcomere is shown during static pacing ($g = 0.0$; Fig. 4A) at 350 ms and alternans control pacing with a target cycle length of 350 ms ($g=1.5$; Fig. 4B and C). The amplitudes of Ca-alternans and APD-alternans are quantified in these simulations by

$$\Delta c(k,n) = (-1)^n (C_n^k - C_{n-1}^k), \tag{18}$$

$$\Delta A(n) = (-1)^n (A_n - A_{n-1}), \tag{19}$$

where C_n^k is the peak Ca concentration of sarcomere k and A_n is the APD of beat n. The sign of Δc and ΔA thus indicates the phase of each alternans, with amplitudes of opposite sign representing alternans of opposite phase. Likewise, at the spatially homogeneous period-1 state, $\Delta A = 0$ and $\Delta c = 0$ for all sarcomeres. The factor $(-1)^n$ is included so that the phase does not alternate on consecutive beats.

Starting from the period-1, spatially homogeneous steady state, during static pacing the Ca transient of every sarcomere begins to alternate in-phase (every sarcomere has a positive Δc) along the length of the cell (Fig. 4A). In contrast, during alternans control pacing a marked gradient in Ca-alternans amplitude (subcellular alternans) develops along the length of the cell, in which the two halves of the cell alternate out of phase (Δc of opposite sign; Fig. 4B and C).

As predicted by the above analysis, subcellular alternans was never induced during static pacing ($g=0.0$) for any of the three models and was not induced in the V_m−driven instability model even during alternans control pacing (not shown). In both the Ca-driven (Fig. 4) and mixed instability model, for all pacing cycle lengths at which alternans was seen during static pacing, alternans control with gain above a low threshold induced subcellular alternans ($g=0.2$–0.4 for the mixed instability model, Fig. 5). The full results of this protocol for the mixed instability model are seen in Fig. 5. Notably, in the mixed instability model, at very fast cycle lengths ($T^* < 230$ ms) alternans control successfully eliminates both APD and Ca-alternans (in every sarcomere) *without* inducing subcellular alternans (discussed below).

4.2. Subcellular alternans is only induced when Ca-cycling dynamics are the primary source of instability

The above theoretical analysis predicts that alternans control pacing will induce subcellular alternans only if Ca-cycling dynamics are more unstable than the APD, consistent with our

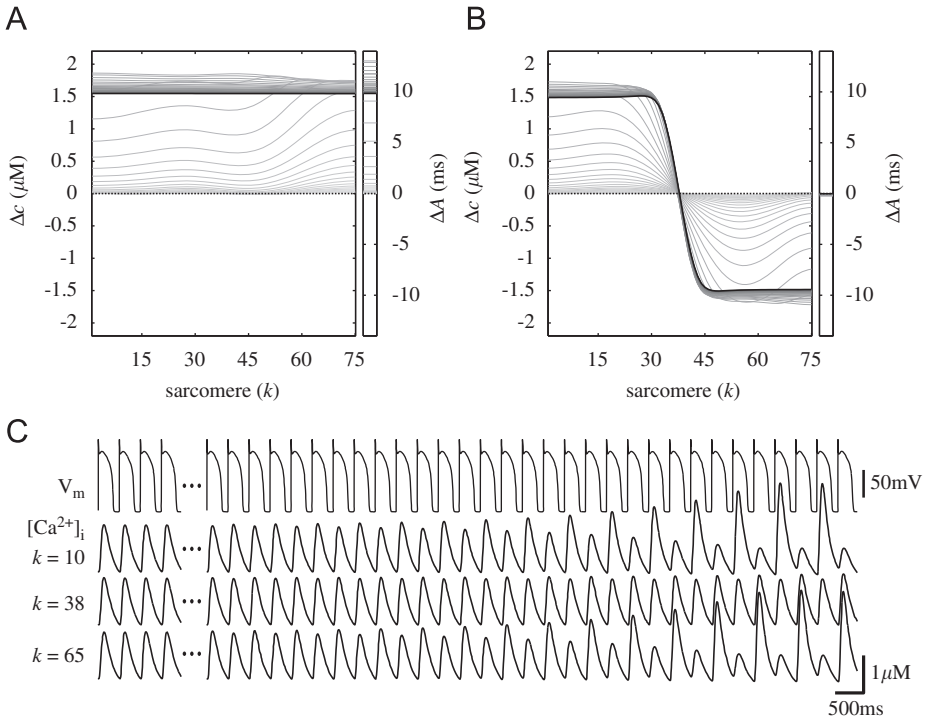


Fig. 4. Starting from the spatially homogeneous, period-1 state ($\Delta c = 0$), the Ca-driven instability cell model was paced for 300 beats (150 of which are shown) (A) with static pacing at cycle length of 350 ms and (B) with alternans control pacing with a target pacing cycle length $T^* = 350$ ms and gain (g) of 1.5. During alternans control pacing (B), a marked subcellular alternans pattern arises, with a period-1 node ($\Delta c = 0$) in the center of the cell. Ca-alternans (Δc) is quantified as $\Delta c = (-1)^n (C_n^k - C_{n-1}^k)$, where C_n^k is the peak $[Ca]_i$ of sarcomere k during beat n. APD-alternans (ΔA) is defined as $\Delta A = (-1)^n (A_n - A_{n-1})$, where A_n is the APD of beat n. The results after 150 beats are indicated as black lines, with snapshots from every two beats included in gray. (C) V_m and $[Ca]_i$ of sarcomeres 10, 38, and 65 of the first 55 beats of the simulation in (B). Beats 5–25 are omitted.

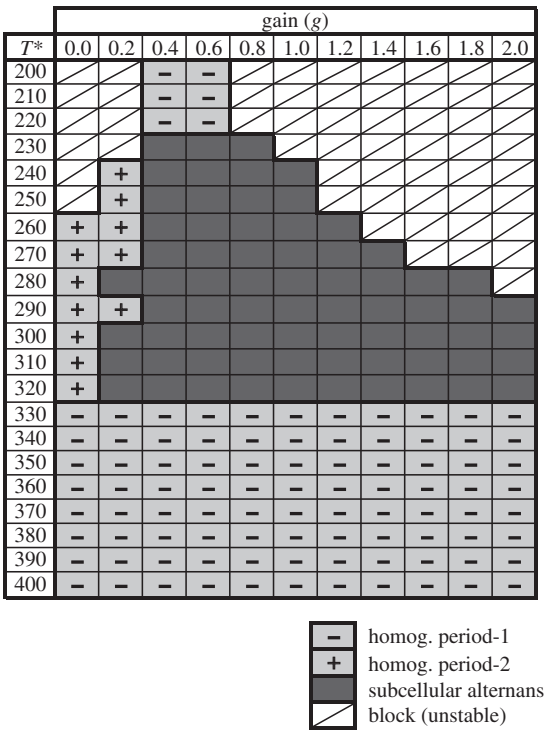


Fig. 5. The effects of alternans control were tested over a range of target cycle lengths (T^*) and control gains (g) in the mixed instability cell model with positive $Ca \rightarrow V_m$ coupling. The results for each simulation are shown, according to the legend above (with the operational definitions below). Subcellular alternans was never seen with static pacing ($g=0.0$). At cycle lengths from 230 to 320 ms, subcellular alternans was induced when alternans control was applied with gain above a low threshold ($g=0.2$–0.4). At cycle lengths less than $T^*=230$ ms, alternans control (with gain of 0.4 and 0.6) successfully eliminated Ca-alternans without inducing subcellular alternans. No alternans (at any scale) was seen at cycle lengths greater than 330 ms. "Homogeneous period-1" and "homogeneous period-2" simulations are defined as those simulations in which the Ca transients of all sarcomeres were spatially homogeneous at the end of the simulation (disregarding the random noise added before each stimulus), with every sarcomere's Ca transients occurring at approximately a period-1 or period-2 rhythm, respectively. See Fig. 4A for an example of a homogeneous period-2 simulation. Simulations labeled as "Subcellular alternans" were those in which smooth gradients of Ca-alternans amplitude were seen at the end of the simulation, with Ca-alternans of opposite phase seen in different subcellular regions (see Fig. 4B and C, for example). "Block" indicates those simulations in which at any point during the 300 beats at least one stimulus was not captured (no AP elicited). See text for a full description of the simulation protocol.

finding that subcellular alternans was not induced in the V_m–driven instability cell model. We further hypothesized that the absence of subcellular alternans during alternans control pacing of the mixed instability model at very fast pacing cycle lengths ($T^* < 230$ ms for $g=0.4$, 0.6; Fig. 5) could be accounted for if there was a cycle length-dependent transition in the primary source of alternans instability (from Ca-driven at slower cycle lengths to V_m–driven at these fast cycle lengths).

Indeed, a previous computational study (Jordan and Christini (2007)) showed that the relative contributions of V_m–driven and Ca-driven instability to the total cellular instability seen during alternans vary at different cycle lengths and likely in different cell types. We implemented the protocol of this previous study (first introduced in Li and Otani, 2003) to find the cycle length dependent contributions of V_m–driven and Ca-cycling instability to the total instability of the mixed-instability cell model, and therefore determine if such a change in stability could account for the rate-dependent subcellular alternans seen in Fig. 5.

Briefly, a finite difference method was used to approximate a mapping matrix (M), relating the state variables at the beginning of each cycle to their values at the beginning of the next. Starting from steady-state (at the spatially homogeneous, period-1 fixed point), each column of M is calculated by perturbing a single state variable a small distance away from its period-1 value (relative perturbation amplitude of 10^{-7}) and measuring the resulting perturbation to all state variables (relative to their steady-state values) precisely one cycle length later. Each of these resulting perturbations is then divided by the size of the initial perturbation to yield the corresponding column of M. This process is repeated for each state variable to define all columns of M. The largest negative eigenvalue of this matrix (λ, referred to as the "alternans eigenvalue" in Li and Otani, 2003) is a measure of the stability of this fixed point, with $|\lambda| < 1$ indicating stable dynamics and $|\lambda| > 1$ indicating unstable dynamics. Note that $\lambda < -1$ indicates unstable, alternating dynamics.

As in Jordan and Christini (2007), implementing this protocol during static pacing yields a measure (λ_{paced}) of the total cellular instability, including contributions from both membrane voltage and Ca-cycling dynamics. By repeating this protocol during a so-called "action potential (AP) clamp", in which the membrane voltage is forced to repeatedly follow the recorded morphology of the model's period-1 AP, the instability measured ($\lambda_{AP\ Clamp}$) reflects the instability of the Ca-cycling dynamics alone. Likewise, during a so-called "Ca clamp", in which intracellular Ca concentrations are forced to repeatedly follow the recorded morphology of the model's period-1 Ca transient (clearly not possible experimentally), the instability measured by this protocol ($\lambda_{Ca\ Clamp}$) is that instability due to membrane voltage dynamics only.

Fig. 6 shows the results for each of these three protocols over a range of cycle lengths in the mixed instability model with positive $Ca \rightarrow V_m$ coupling, allowing inspection of the cycle length dependent contributions of V_m and Ca-cycling dynamics to the total instability. As in the non-spatially extended version of this model used in Jordan and Christini (2007) (referred to as the "SSK" model in this previous study), the total instability of the cell is seen to become unstable ($\lambda_{paced} < -1$, indicating alternans will

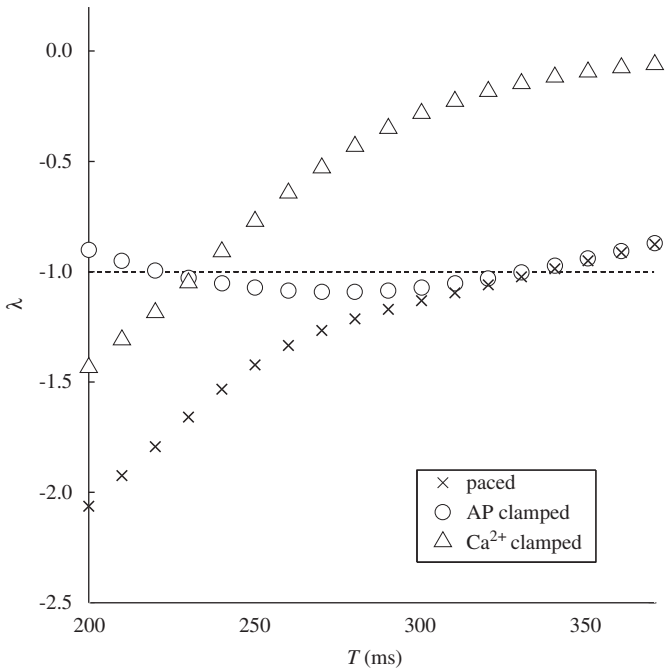


Fig. 6. Using the technique of Jordan and Christini (2007) and Li and Otani (2003), the instability due to membrane voltage dynamics ($\lambda_{Ca\ Clamp}$, △), Ca-cycling dynamics ($\lambda_{AP\ Clamp}$, ○) and the total instability (λ_{paced}, ×) were found for the cycle lengths shown, with $|\lambda| < 1$ indicating stable dynamics and $|\lambda| > 1$ indicating unstable dynamics. See text for detailed description of protocol.

occur) at cycle lengths less than 330 ms. At cycle lengths greater than 230 ms, $|\lambda_{\text{AP Clamp}}| > |\lambda_{\text{Ca Clamp}}|$, indicating that Ca-cycling dynamics are more unstable than membrane voltage dynamics (alternans is Ca-driven) at these cycle lengths. At shorter cycle lengths, however, V_m–driven instability becomes greater than Ca-cycling instability ($|\lambda_{\text{Ca Clamp}}| > |\lambda_{\text{AP Clamp}}|$; V_m–driven alternans), corresponding to those cycle lengths in Fig. 5 in which alternans control pacing successfully eliminates alternans without inducing subcellular alternans ($T^* < 230$ ms for $g=0.4$, 0.6). This supports our hypothesis that the rate-dependent presence or absence of subcellular alternans seen during alternans control pacing in this model was due to a rate-dependent transition in the primary source of instability.

4.3. The computed stability spectrum is consistent with analytical predictions

To further compare our results with analytical predictions, we compared the numerically computed stability spectrum for the ionic cell model during alternans control pacing with that (found previously) for the simplified reaction–diffusion model (Eq. (7)). Note once again that alternans control pacing does not change the structure of either the 2D sarcomere model or these derived amplitude equations, and thus the same stability spectrum is predicted during alternans control pacing.

Linear stability analysis of the derived amplitude equations (Eq. (7)) in Shiferaw and Karma (2006) found the stability of this model in the presence of sinusoidal perturbations in Ca-alternans amplitude (with wavelength $2\pi/q$) to be

$$\Omega(q) = \delta - q^2 D, \tag{20}$$

where δ and D are the coefficients of the whole cell reaction diffusion model, as above (Eq. (7)). As detailed in Shiferaw and Karma (2006), $\delta = (J_{22}^2 - 1)/2T$ and D is dependent on the diffusion constant of intracellular Ca, the pacing period, and J_{22}.

To compare the stability of the ionic model with this prediction, we measured the growth rate of Ca-alternans during alternans control pacing, following the addition of small sinusoidal perturbations to the Ca concentrations (and therefore Ca-alternans magnitudes) of each sarcomere in a 400 sarcomere model cell (as in Shiferaw and Karma, 2006). By calculating this growth rate for a range of perturbation wavelengths and with a range of alternans control gains, we were able to compute the stability spectrum for this model, seen in Fig. 7. These simulations were performed in the Ca-driven alternans model with positive $Ca \rightarrow V_m$ coupling.

For each simulation, a model cell was initialized to its period-1 homogeneous conditions (as above) and small amplitude (approximately 1% of steady-state Ca concentrations) sinusoidal perturbations were added to intracellular calcium concentrations with a wavelength of $\lambda = 2\pi/q$, where $q = k\pi/L$ (for cell length L and $k=\{1,2,3,\ldots 30\}$). On the same beat as these sinusoidal perturbations were added, alternans control pacing (using Eq. (8)) was initiated. For each perturbation wavelength, alternans control gains of 0.0–2.0 were tested at a target pacing cycle length of $T^* = 350$ ms. The growth rate of these perturbations was calculated (as in Shiferaw and Karma, 2006) as the slope of the linear-log plot of the root mean square of the average Ca-alternans magnitude (defined as $C(n) = [1/N\sum_{k=1,N}\Delta c(k,n)^2]^{1/2}$) versus time $t=nT$.

Pattern formation is predicted to occur when the growth rate of the homogeneous state ($\Omega(0)$) is less than the growth rate of the fastest growing sinusoidal perturbation (which by Eq. (20) will be $\lim \Omega(q)_{q\rightarrow 0} = \delta$). Note that the definition of $\Omega(q)$ does not contain any diastolic interval-dependent terms, and is therefore predicted to be unchanged during alternans control pacing. As such, alternans control is predicted to induce pattern formation by stabilization of the homogeneous state to below the stability of the system when diffusion is present.

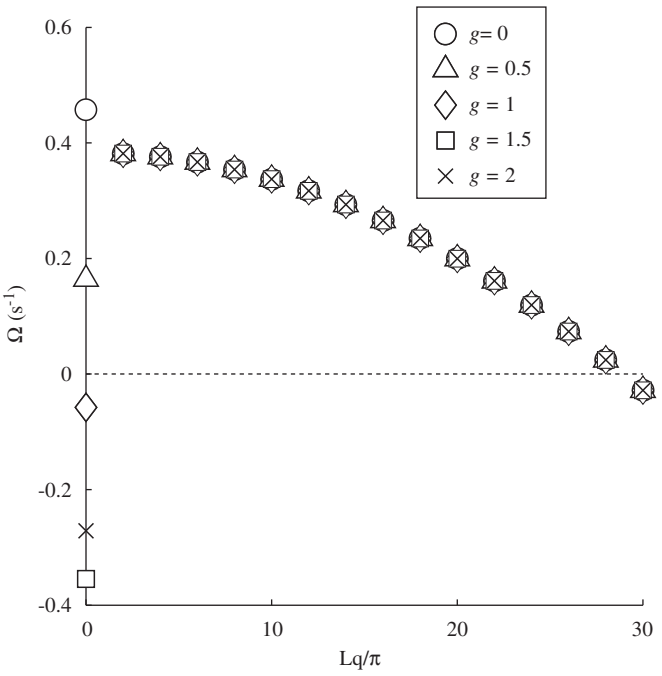


Fig. 7. The growth rate (Ω) of Ca-alternans during alternans control pacing (with gain g) was computed after the addition of sinusoidal perturbations to Ca concentrations with wavelength $\lambda = 2\pi/q$. Here the growth rates are plotted as a function of the dimensionless wavenumber Lq/π. Subcellular alternans is predicted to occur when $\Omega(0) < \lim\Omega(q)_{q\rightarrow 0}$, seen here to occur at a gain between 0.0 and 0.5. As predicted, the magnitude of alternans control gain affects only the stability of the homogeneous state.

The calculated stability spectrum seen in Fig. 7 is consistent with the predictions of the above analysis. Varying the gain of control has little effect on the growth rate of sinusoidal perturbations in Ca-alternans ($\Omega(q)$) but strongly influences the stability of the spatially homogeneous state ($\Omega(0)$). This is due to the spatially uniform APD (secondary to an assumption of instantaneous voltage diffusion), which dictates that the effects of intracellular Ca transients on the APD ($Ca \rightarrow V_m$ coupling) are averaged over all sarcomeres. In the presence of the added sinusoidal perturbations in Ca-transients, therefore, the APD-prolonging and APD-shortening effects of the perturbed Ca-transients are balanced, and the APD remains at period-1 (as would be expected in a real cell). During a period-1 APD, alternans control pacing (Eq. (8)) does not perturb the cycle length, and thus does not have an effect on the stability of the cell model. APD-alternans is seen, however, in the presence of spatially homogeneous perturbations in Ca-transients ($Lq/\pi = 0$), causing alternans control pacing to perturb the pacing cycle length of the cell model and decrease its instability ($\Omega(0)$). During static pacing ($g=0$), pattern formation is not predicted by this dispersion relationship ($\Omega(0) > \lim\Omega(q)_{q\rightarrow 0}$) and indeed subcellular alternans is not seen. Furthermore, the gain at which $\Omega(0) < \lim\Omega(q)_{q\rightarrow 0}$ (between $g=0.0$ and 0.5), corresponds to the gain at which subcellular alternans was induced in these simulations as well as in the simulations above (in which alternans control pacing was tested in the presence of random noise).

5. Discussion

Subcellular alternans, in which Ca-alternans occurs with opposite phase in adjacent regions within an individual myocyte,

has been frequently reported in the recent literature, in both isolated myocytes (Kockskämper and Blatter, 2002; Díaz et al., 2004, 2002; Cordeiro et al., 2007; Karma and Gilmour, 2007; Gaeta et al., 2009) as well as within individual myocytes of the intact heart (Aistrup et al., 2006, 2009; Kapur et al., 2009; Xie and Weiss, 2009), but it remains poorly characterized. Although this phenomenon has been most often reported in isolated myocytes following the application of drugs that increase subcellular heterogeneity (Díaz et al., 2002, 2004; Kockskämper and Blatter, 2002), subcellular alternans has also been reported in otherwise healthy cells during rapid, static pacing (Kockskämper and Blatter, 2002; Cordeiro et al., 2007). Whereas the former studies are likely to be most relevant to the particular disease states that they model, we believe the latter, pacing-induced subcellular alternans represents previously uncharacterized physiologic myocyte dynamics that are likely to play a role in any context.

Subcellular alternans can be understood as the formation of a pattern in subcellular Ca transients from an initially (approximately) spatially homogeneous state. A fundamental question when studying any such pattern formation is whether the patterns reflect the presence of preexisting heterogeneities of the substrate in question (as proposed in Aistrup et al., 2009), dynamically induced heterogeneity (as proposed in Xie and Weiss, 2009; Shiferaw and Karma, 2006), or a combination of the two. We recently showed that subcellular alternans is robustly induced during alternans control pacing of isolated guinea pig ventricular myocytes, suggesting that it can indeed be induced by a dynamical mechanism (Gaeta et al., 2009). Here we show analytically that this observation can be accounted for by a previously proposed dynamical mechanism, in which proper bidirectional coupling between the APD and the Ca transient induces subcellular alternans formation by a Turing-type, pattern forming instability (Shiferaw and Karma, 2006).

The proposed mechanism essentially states that for a pattern to form, local activation must be coupled to long-range inhibition (Meinhardt and Gierer, 2000). In the previously proposed analogy, Ca-alternans fulfills the role of the local, autocatalytic activator and APD-alternans the role of the more quickly diffusing inhibitor (as described in Shiferaw and Karma, 2006). To form subcellular alternans, a local increase in Ca-alternans must produce APD-alternans that will inhibit Ca-alternans at distant subcellular locations. Such dynamics are possible only if the secondary APD-alternans generated by the local Ca-alternans are either (A) out-of-phase with the original Ca-alternans or (B) in-phase with the local Ca-alternans, but induce out-of-phase Ca-alternans at other subcellular sites. Whereas the former mechanism requires negative $Ca \rightarrow V_m$ coupling (to switch the phase of secondary APD-alternans) and positive $V_m \rightarrow Ca$ coupling (so that the phase is not switched back when the APD-alternans generates secondary Ca-alternans), the latter mechanism corresponds to our proposed mechanism, in which $Ca \rightarrow V_m$ coupling is positive but $V_m \rightarrow Ca$ coupling is negative.

Because graded release ensures positive $V_m \rightarrow Ca$ coupling during static pacing, subcellular alternans was previously predicted to occur during static pacing only in those cells with negative $Ca \rightarrow V_m$ coupling (and Ca-driven alternans) (Shiferaw and Karma, 2006). For subcellular alternans to be formed by this mechanism in myocytes with positive $Ca \rightarrow V_m$ coupling, however, $V_m \rightarrow Ca$ coupling must be negative, which has never been experimentally reported. Here we have shown that during alternans control pacing, with gain above a low threshold ($g > 1$ in the coupled map model), $V_m \rightarrow Ca$ coupling is effectively negative, thereby predicting that alternans control pacing will induce subcellular alternans in cardiac myocytes with positive $Ca \rightarrow V_m$ coupling (and Ca-driven alternans). We believe that this dynamical mechanism accounts for our previous observation of subcellular alternans during alternans control pacing of isolated guinea pig ventricular myocytes (Gaeta et al., 2009). Additionally, as detailed in Gaeta et al. (2009), this same mechanism may also contribute to subcellular alternans seen during static pacing of intact tissue, in which conduction velocity restitution can lead to alternans control-like effects on the cycle lengths of cells distant from the pacing site.

Note that although we believe this work strongly supports the proposed Turing-type instability as a possible mechanism of subcellular alternans, it does not rule out a possible contribution by other proposed anatomical and dynamical sources of heterogeneity. It is likely that a rich interplay of both dynamical and anatomical factors contribute to this phenomenon *in vivo*.

The above theoretical analysis additionally predicts that subcellular alternans can only occur if Ca-cycling dynamics are more unstable than the APD. Intuitively, if this were not the case, the spatially uniform APD-alternans would simply drive in-phase Ca-alternans everywhere in the cell (through $V_m \rightarrow Ca$ coupling; Shiferaw and Karma, 2006). This prediction is supported by our finding in the ionic cell model that alternans control pacing never induced subcellular alternans in either the V_m−driven instability model or in the mixed-instability model at cycle lengths at which V_m−driven instability is greater than Ca-driven instability ($T^* < 230$ ms; Fig. 5).

This raises the intriguing possibility that alternans control pacing can be used as an experimental tool to determine if/when Ca-cycling dynamics are indeed the primary source of instability (as is normally assumed). Systematic application of alternans control pacing over a range of pacing cycle lengths can be used to test for the primary source of instability and to determine if this is a rate and/or cell-type dependent property in real cells as in the cell model studied here. We further speculate that perhaps such a rate dependent transition in the primary source of instability could contribute to previous reports of subcellular alternans in which spatially concordant Ca-alternans at slower cycle lengths transitioned to subcellular alternans with rapid pacing (Aistrup et al., 2006, 2009; Cordeiro et al., 2007; Kapur et al., 2009).

Finally, as described in Shiferaw and Karma (2006), we note that the proposed mechanism for subcellular alternans provides a rare example of a Turing instability in a biological system in which the diffusing morphogens are readily identified. We hope that in addition to its utility in the study of subcellular alternans itself, the analytical and experimental approach identified here (in concert with Shiferaw and Karma, 2006; Gaeta et al., 2009) will instigate future studies of biological pattern formation in this relatively simple model system.

5.1. Limitations

It is notable that the coupled map model analysis predicts that a control gain $g > 1$ is necessary for $V_m \rightarrow Ca$ coupling to become negative and thus subcellular alternans to occur, whereas in the ionic model and our experiments (Gaeta et al., 2009) such a transition occurs at a much lower gain threshold ($g = 0.2$–0.4 in the model). Below, we argue that the exaggerated threshold may arise from the fact that our analysis dealt only with changes to the diastolic interval; the discrepancy can be accounted for by also including the separate effect of the cycle length on recovery of Ca-cycling dynamics.

If $V_m \rightarrow Ca$ coupling is mediated by changes to the diastolic interval (as is assumed in the above analysis), for negative $V_m \rightarrow Ca$ coupling the gain of alternans control must be large enough to perturb the diastolic interval beyond its period-1 duration. Given, for example, an increase in APD, if $g = 1$, alternans control extends the diastolic interval by precisely the amount that

would be lost by such an increase in APD during static pacing and the Ca transient would be unchanged. Likewise, $g<1$ would cause a smaller than period-1 diastolic interval and subsequent Ca transient and therefore positive $V_m \rightarrow Ca$ coupling is preserved ($\partial C_n/\partial A_{n-1}<0$). Only with $g>1$ will an increase in the APD extend the diastolic interval beyond its period-1 duration and a larger than period-1 subsequent Ca transient result (negative $V_m \rightarrow Ca$ coupling ($\partial C_n/\partial A_{n-1}>0$)).

The analytical and computational results can be reconciled if several differences between the coupled map and the ionic model are considered. First, the cycle length is not explicitly included in the simple 2-dimensional map. Rather, we have only included the effects of alternans control on diastolic interval, not the effect on cycle length that is clearly present in a real paced cell (and the ionic model; as seen in Fig. 3). Although diastolic interval-dependent processes (such as graded release and APD restitution) can be accounted for with this approximation, SR Ca reuptake (among other Ca-cycling dynamics) is independent of membrane voltage and is better approximated as a cycle length dependent process (as in Qu et al., 2007; Shiferaw et al., 2003; Mahajan et al., 2008). Because the size of each Ca transient is steeply dependent on the SR Ca content (Bassani et al., 1995; Díaz et al., 2004), the cycle length changes during alternans control will have important effects on Ca-cycling dynamics that are not included in the above analysis. Prolonging the preceding cycle length, for example, will allow greater time for SR Ca-reuptake and therefore increased SR Ca-content at the time of the next release. Because of the strong dependence of the magnitude of each Ca transient on the SR Ca-content (Díaz et al., 2004; Bassani et al., 1995), this will lead to a larger Ca transient (and therefore $\partial C_n/\partial T_{n-1}>0$).

This dependence can be included in the 2-dimensional map by expanding the dependence of each Ca transient on the preceding APD to include both a diastolic interval dependence (graded release) and a cycle-length dependence (SR Ca reuptake). Including this relationship lowers the gain threshold above which negative $V_m \rightarrow Ca$ coupling (and thus subcellular alternans) is predicted to occur, as follows.

With this cycle length dependence of the Ca transient, $V_m \rightarrow Ca$ coupling is defined (from Eq. (4)) as

$$\frac{\partial C_n}{\partial A_{n-1}} \equiv \frac{\partial C_n}{\partial d_{n-1}}\frac{\partial d_{n-1}}{\partial A_{n-1}} + \frac{\partial C_n}{\partial T_{n-1}}\frac{\partial T_{n-1}}{\partial A_{n-1}}, \tag{21}$$

noting that $\partial d_n/\partial A_n = g-1$ and $\partial T_n/\partial A_n = g$ during alternans control (from Eq. (8)), this becomes

$$\frac{\partial C_n}{\partial A_{n-1}} \equiv (g-1)\frac{\partial C_n}{\partial d_{n-1}} + (g)\frac{\partial C_n}{\partial T_{n-1}}, \tag{22}$$

with this added cycle length dependence, $V_m \rightarrow Ca$ coupling therefore becomes negative ($\partial C_n/\partial A_{n-1}>0$) when

$$g\left(\frac{\partial C_n}{\partial d_{n-1}} + \frac{\partial C_n}{\partial T_{n-1}}\right) > \frac{\partial C_n}{\partial d_{n-1}}. \tag{23}$$

Noting that $\partial C_n/\partial T_{n-1}>0$ and $\partial C_n/\partial d_{n-1}>0$ (as described above), we see that $g>1$ is a sufficient, but not necessary condition. The gain threshold for negative $V_m \rightarrow Ca$ coupling will be lowered as the steepness of the cycle length dependence of Ca-release increases. Physiologically, this dependence will be influenced by both the load dependence of SR Ca-release and the efficiency of SR Ca reuptake. For example, the steeper the load dependence of SR Ca-release (increasing $\partial C_n/\partial T_{n-1}$), the lower will be the alternans control gain threshold for negative $V_m \rightarrow Ca$ coupling.

Incorporating this cycle length dependence in Ca-cycling dynamics therefore lowers the alternans control gain threshold above which subcellular alternans is predicted, and brings the analytical predictions closer to those seen in the ionic model and experimental studies (Gaeta et al., 2009).

Acknowledgments

This work was supported by NIH Medical Scientist Training Program Grant GM07739 (to S.A.G.), NIH Grant 1 F30 HL095324-01 (to S.A.G.), NIH Grant 1R01HL094620 (to D.J.C.), and the Kenny Gordon Foundation.

References

Aistrup, G.L., Kelly, J.E., Kapur, S., Kowalczyk, M., Sysman-Wolpin, I., Kadish, A.H., Wasserstrom, J.A., 2006. Pacing-induced heterogeneities in intracellular ca2+ signaling, cardiac alternans, and ventricular arrhythmias in intact rat heart. Circ. Res. 99 (7), e65–e73.

Aistrup, G.L., Shiferaw, Y., Kapur, S., Kadish, A.H., Wasserstrom, J.A., 2009. Mechanisms underlying the formation and dynamics of subcellular calcium alternans in the intact rat heart. Circ. Res. 104 (5), 639–649.

Bassani, J.W., Yuan, W., Bers, D.M., 1995. Fractional sr ca release is regulated by trigger ca and sr ca content in cardiac myocytes. Am. J. Physiol. 268 (5 Pt 1), C1313–C1319.

Cheng, H., Lederer, W.J., 2008. Calcium sparks. Physiol. Rev. 88 (4), 1491–1545.

Christini, D.J., Riccio, M.L., Culianu, C.A., Fox, J.J., Karma, A., Gilmour, R.F., 2006. Control of electrical alternans in canine cardiac purkinje fibers. Phys. Rev. Lett. 96 (10), 104101.

Cordeiro, J.M., Malone, J.E., Diego, J.M.D., Scornik, F.S., Aistrup, G.L., Antzelevitch, C., Wasserstrom, J.A., 2007. Cellular and subcellular alternans in the canine left ventricle. Am. J. Physiol. Heart Circ. Physiol. 293 (6), H3506–H3516.

Díaz, M.E., Eisner, D.A., O'Neill, S.C., 2002. Depressed ryanodine receptor activity increases variability and duration of the systolic ca2+ transient in rat ventricular myocytes. Circ. Res. 91 (7), 585–593.

Díaz, M.E., O'Neill, S.C., Eisner, D.A., 2004. Sarcoplasmic reticulum calcium content fluctuation is the key to cardiac alternans. Circ. Res. 94 (5), 650–656.

Euler, D.E., 1999. Cardiac alternans: mechanisms and pathophysiological significance. Cardiovasc. Res. 42 (3), 583–590.

Franzini-Armstrong, C., Peachey, L.D., 1981. Striated muscle-contractile and control mechanisms. J. Cell Biol. 91 (3 Pt 2), 166s–186s.

Gaeta, S.A., Bub, G., Abbott, G.W., Christini, D.J., 2009. Dynamical mechanism for subcellular alternans in cardiac myocytes. Circ. Res. 105 (4), 335–342.

Gierer, A., Meinhardt, H., 1972. A theory of biological pattern formation. Kybernetik 12 (1), 30–39.

Hall, G.M., Gauthier, D.J., 2002. Experimental control of cardiac muscle alternans. Phys. Rev. Lett. 88 (19), 198102.

Hall, K., Christini, D.J., 2001. Restricted feedback control of one-dimensional maps. Phys. Rev. E 63 (4), 046204. doi:10.1103/PhysRevE.63.046204.

Jordan, P.N., Christini, D.J., 2007. Characterizing the contribution of voltage- and calcium-dependent coupling to action potential stability: implications for repolarization alternans. Am. J. Physiol. Heart Circ. Physiol. 293 (4), H2109–H2118.

Kapur, S., Wasserstrom, J.A., Kelly, J.E., Kadish, A.H., Aistrup, G.L., 2009. Acidosis and ischemia increase cellular ca2+ transient alternans and repolarization alternans susceptibility in the intact rat heart. Am. J. Physiol. Heart Circ. Physiol. 296 (5), H1491–H1512.

Karma, A., Gilmour, R., 2007. Nonlinear dynamics of heart rhythm disorders. Phys. Today 60 (3), 51.

Kockskämper, J., Blatter, L.A., 2002. Subcellular ca2+ alternans represents a novel mechanism for the generation of arrhythmogenic ca2+ waves in cat atrial myocytes. J. Physiol. (Lond.) 545 (Pt 1), 65–79.

Li, M., Otani, N.F., 2003. Ion channel basis for alternans and memory in cardiac myocytes. Ann. Biomed. Eng. 31 (10), 1213–1230.

Mahajan, A., Shiferaw, Y., Sato, D., Baher, A., Olcese, R., Xie, L.-H., Yang, M.-J., Chen, P.-S., Restrepo, J.G., Karma, A., Garfinkel, A., Qu, Z., Weiss, J.N., 2008. A rabbit ventricular action potential model replicating cardiac dynamics at rapid heart rates. Biophys. J. 94 (2), 392–410.

Meinhardt, H., Gierer, A., 2000. Pattern formation by local self-activation and lateral inhibition. Bioessays 22 (8), 753–760.

Murray, J., 2003. Mathematical Biology. Springer Verlag.

Narayan, S., 2006. T-wave alternans and the susceptibility to ventricular arrhythmias. J. Am. College Cardiol. 47 (2), 269–281.

Pastore, J.M., Girouard, S.D., Laurita, K.R., Akar, F.G., Rosenbaum, D.S., 1999. Mechanism linking t-wave alternans to the genesis of cardiac fibrillation. Circulation 99 (10), 1385–1394.

Qu, Z., Shiferaw, Y., Weiss, J., 2007. Nonlinear dynamics of cardiac excitation–contraction coupling: an iterated map study. Phys. Rev. E 75, 011927-01–011927-13.

Qu, Z., Weiss, J.N., 2007. The chicken or the egg? Voltage and calcium dynamics in the heart. Am. J. Physiol. Heart Circ. Physiol. 293 (4), H2054–H2055. doi:10.1152/ajpheart.00830.2007.

Rubenstein, D.S., Lipsius, S.L., 1995. Premature beats elicit a phase reversal of mechanoelectrical alternans in cat ventricular myocytes. A possible mechanism for reentrant arrhythmias. Circulation 91 (1), 201–214.

Shiferaw, Y., Karma, A., 2006. Turing instability mediated by voltage and calcium diffusion in paced cardiac cells. Proc. Natl. Acad. Sci. USA 103 (15), 5670–5675.
Shiferaw, Y., Sato, D., Karma, A., 2005. Coupled dynamics of voltage and calcium in paced cardiac cells. Phys. Rev. E Stat. Nonlin. Soft Matter Phys. 71 (2 Part 1), 021903.
Shiferaw, Y., Watanabe, M.A., Garfinkel, A., Weiss, J.N., Karma, A., 2003. Model of intracellular calcium cycling in ventricular myocytes. Biophys. J. 85 (6), 3666–3686.
Turing, A.M., 1952. The chemical basis of morphogenesis. Philos. Trans. R. Soc. Lond. Ser. B Biol. Sci. 237 (641), 37–72.
Weiss, J.N., Karma, A., Shiferaw, Y., Chen, P.-S., Garfinkel, A., Qu, Z., 2006. From pulsus to pulseless: the saga of cardiac alternans. Circ. Res. 98 (10), 1244–1253.
Xie, L., Weiss, J.N., 2009. Arrhythmogenic consequences of intracellular calcium waves. Am. J. Physiol. Heart Circ. Physiol. 297 (3), H997-H1002. doi:10.1152/ajpheart.00390.2009.